UTX Epigenetically Imposes a Cytolytic Effector Program in Autoreactive Stem-like CD8+ T cell Progenitors

Authors: Ho-Chung Chen[1], Hsing Hui Wang[2], Lisa A. Kohn[3], David Sailer[2], Shirley Zhang[4], Ethan McCarthy[1], Maryam Seyedsadr[1], Zikang Zhou[1], Xihui Yin[5], Nicole Wilkinson[1], Jessica Ortega[3], Melissa G. Lechner[3]*, Willy Hugo[3]*, Maureen A. Su[1,6,7]*

Affiliations:

1. Department of Microbiology, Immunology, and Molecular Genetics, UCLA David Geffen School of Medicine; Los Angeles, CA 90095.
2. Department of Pediatrics, UNC Chapel Hill, Chapel Hill, NC, 27599
3. Department of Medicine, UCLA David Geffen School of Medicine; Los Angeles, CA 90095.
4. Department of Molecular and Medical Pharmacology, UCLA David Geffen School of Medicine; Los Angeles, CA 90095.
5. Department of Biology, Massachusetts Institute of Technology, Boston, MA 02139
6. Department of Pediatrics, UCLA David Geffen School of Medicine; Los Angeles, CA 90095.
7. Lead contact

*Corresponding authors:

Maureen A. Su, Email: masu@mednet.ucla.edu

Willy Hugo, Email: hwilly@mednet.ucla.edu

Melissa G. Lechner, Email: mlechner@mednet.ucla.edu

Summary

Type 1 Diabetes Mellitus (T1D) is an autoimmune disease caused by unremitting immune attack on pancreas insulin-producing beta cells. Persistence of the autoimmune response is mediated by TCF1+ Ly108+ progenitor CD8+ T (T_{prog}) cells, a stem-like population that gives rise to exhausted effectors with limited cytolytic function in chronic virus infection and cancer. What paradoxically drives T_{prog} conversion to highly cytolytic effectors in T1D, however, remains unclear. Here, we show that the epigenetic regulator UTX controls diabetogenic CD8+ T_{prog} differentiation by poising chromatin for transition to a cytolytic effector state. Indeed, deletion of UTX function in T cells impairs conversion of T_{prog} to autoimmune effectors and protects mice from spontaneous diabetes, as well as an aggressive form of autoimmune diabetes induced by anti-PD1 cancer immunotherapy. Furthermore, short-term treatment with UTX inhibitor GSKJ4 similarly protects from T1D, highlighting the therapeutic potential of targeting UTX-mediated mechanisms to break unremitting autoimmune responses.

Introduction

Type 1 Diabetes (T1D) is an autoimmune disease in which insulin-producing beta cells are destroyed by a sustained T cell attack[1]. As a consequence, clinical symptoms do not remit, and patients require lifelong exogenous insulin administration. This is in contrast to Guillain Barre Syndrome, acute disseminated encephalomyelitis, and other self-limited autoimmune conditions in which the immune response wanes and clinical symptoms usually resolve within months. What underlies autoimmune persistence in T1D is not completely understood and identifying mechanisms that perpetuate chronic immune-mediated destruction is an important step toward developing therapeutic approaches that interrupt this process.

The immune responses in T1D, chronic virus infection, and progressive cancer share multiple overlapping features, including continued T cell activation by persistent antigens and prominence of a long-lived CD8+ T cell stem-like progenitor (T_{prog}) population[2-4]**.** In all three scenarios, TCF1+ Ly108+ T_{prog} cells mediate immune persistence by their continual replenishment of the pool of terminally differentiated CD8+ T cells. At the same time, critical differences also exist between these immune responses. In both chronic virus infection and progressive cancers, T_{prog} cells give rise to CD8+ T cell effector populations that become exhausted and fail to eradicate the immune threat[5,6]. In T1D, on the other hand, T_{prog} cells give rise to CD8+ T cell effectors that retain their autoimmune mediator function and aggressively destroy beta cells[3]. Thus, the chronic immune responses in these three contexts have shared, yet distinct, features.

Epigenetic regulation has been reported to play a key role in governing T_{prog} cell differentiation to an exhausted fate in chronic infection and cancer[7-9]. Because the overlap between these conditions and T1D is only partial, whether epigenetic regulation also governs T_{prog} differentiation to cytolytic effectors in T1D is not clear. Therapies that modulate epigenetic mechanisms are a potent class of drugs already in clinical use for cancer[10] but have not yet been used for T1D or other autoimmune diseases. Here, we show that T_{prog} to cytolytic effector

conversion in T1D is controlled by the epigenetic regulator UTX. Moreover, blockade of UTX function, using genetic and inhibitor-based approaches, protected against T1D, suggesting that UTX-mediated epigenetic mechanisms may be targeted in patients with T1D for therapeutic benefit.

Results

UTX in T cells of NOD mice is required for T1D and alters CD8+ T cell subset distribution.

The epigenetic regulator UTX has been implicated in controlling T cell differentiation in anti-cancer and anti-viral immunity, including upregulation of inhibitory receptors that enforce exhaustion and prevent eradication of cancer or infected cells[8,9,11]. Yet, UTX's role in diabetogenic T cell responses, in which autoreactive T cells actively kill pancreatic insulin-producing beta cells[3], is unknown. To address this, we generated NOD mice with T cell-specific UTX deficiency (*UTX$^{fl/fl}$ Lck-Cre+,* herein referred to as *NOD-UTX^{TCD}*). By 30 weeks of age, none of the *NOD-UTX^{TCD}* female mice were diabetic, in contrast to almost 80% of UTX-sufficient *NOD-WT* littermate controls (UTX T cell-sufficient mice; *UTX$^{fl/fl}$ Lck-Cre-*) **(Fig. 1A)**. Hematoxylin/eosin (H/E) stained pancreas sections showed significantly reduced immune infiltration in the islets of *NOD-UTX^{TCD}* mice, compared to *NOD-WT* controls (**Fig. 1B, C**). Thus, T cell-specific UTX deficiency protects against diabetes and insulitis in NOD mice.

We next explored the cellular mechanism by which T cell-specific UTX deficiency protects from T1D. Prior to infiltrating pancreatic islets, diabetogenic CD4+ and CD8+ T cells are first primed in the pancreatic lymph nodes (pLN)[3,12]. To delineate how UTX deficiency alters T cell dynamics in pLN of NOD mice, therefore, we performed single cell RNA seq (scRNAseq) of pLN immune cells (CD45+) from 8 and 13 week old *NOD-WT* and *NOD-UTX^{TCD}* mice (**Fig. 1D**; n=6 per genotype). These ages represent distinct stages in T1D autoimmunity development: 8 weeks represents a stage when immune cell infiltration is prominent in islets, and 13 weeks

represents a stage immediately prior to overt diabetes[13]. UMAP clustering of 97,400 cells showed 7 major immune cell populations including CD8+ T cells, CD4+ T cells, B cells, and myeloid cells **(Fig. 1E, Table S1).** Because primary alterations in mice with T cell-specific UTX deletion would be expected to occur in T cell populations, we then further evaluated CD4+ and CD8+ T cell populations. Sub-clustering of CD4+ T cells yielded 10 populations **(Figure S1A)**, including T follicular helper (Tfh) and regulatory T (Treg) cells. *NOD-WT* vs. *NOD-UTX^{TCD}* mice have similar frequencies of key autoimmunity-associated CD4+ T cell subsets in the pLN **(Figure S1B)**. Moreover, flow cytometric analysis of pLN showed similar frequencies of CD4+ T cell subsets [T helper 1 (Th1; IFNg+), Tfh (CXCR5+ PD1+), and Treg (FOXP3+ CD25+)] between *NOD-WT* vs. *NOD-UTX^{TCD}* mice **(Figure S1C)**. Thus, pLN CD4+ T cell distribution was largely unchanged by T cell specific UTX deficiency in NOD mice.

In contrast, significant changes were noted in the distribution of CD8+ T cell subsets between *NOD-WT* and *NOD-UTX^{TCD}* mice. CD8+ T cells sub-clustered into 8 populations (**Fig. 1F**), which included a "CD8+ T_{prog}-like" population that expressed genes associated with stem-like autoimmune progenitor cells (*Tcf7, Slamf6* [which encodes Ly108]*, Sell, Myb, Ikzf2, Id3*) **(Fig. 1G** and **Figure S1E)** and a "CD8+ T_{med}-like" population that expressed genes associated with terminally-differentiated effectors (*Nkg7, Cxcr6, Thy1*)[3,14] **(Fig. 1G)**. Strikingly, a higher frequency of CD8+ T_{prog}-like, and a lower frequency of CD8+ T_{med}-like, cells were seen in the pLN of *NOD-UTX^{TCD}* mice, compared to *NOD-WT* littermates **(Fig. 1H).** Thus, protection from T1D in *NOD-UTX^{TCD}* mice is associated with an altered distribution of pLN CD8+ T cells subsets expressing markers of stem-like progenitors and effectors.

UTX in T cells promotes CD8+ T cell transition from progenitor to cytolytic effector state in T1D

Within the pLN of NOD mice, stem-like progenitors (T_{prog}) have been reported to differentiate into terminally-differentiated autoimmune mediators (T_{med}), which then enter the pancreatic islets to destroy beta cells[3]. In line with this report, pseudotime trajectory analysis of our scRNAseq

dataset suggested a differentiation pathway that starts with the CD8+ T_{prog}-like population, moves through an intermediate population (CD8+ T Intermediate), and ends in the CD8+ T_{med}-like population (**Fig. 2A**). Along the pseudotime axis, expression of stem-like progenitor-associated genes (*Tcf7*, *Slamf6*) was highest in CD8+ T_{prog}-like, decreased in the CD8+ T Intermediate, and lowest in CD8+ T_{med}-like cells **(Fig. 2B, C).** On the other hand, expression of effector-associated genes (*Thy1, Cxcr6*) was lowest in the CD8+ T_{prog}-like, and increased in CD8T-Intermediates and CD8+ T_{med}-like cells **(Fig. 2B, C)**. Of note, T cell-specific UTX deficiency altered this differentiation trajectory. Comparison of cell densities along the pseudotime trajectory revealed relative accumulation of *NOD-UTX*^{TCD} CD8+ T_{prog}-like compared to *NOD-WT*, along with a relative lack of in *NOD-UTX*^{TCD} CD8+ T_{med}-like cells compared to *NOD-WT* (**Fig. 2D).** This difference in differentiation trajectories suggests a potential block in conversion of T_{prog} to T_{med} cells in *NOD-UTX*^{TCD} mice.

We next sought to verify this finding by flow cytometric analysis, using reciprocal expression of Ly108 (*Slamf6*) and CXCR6 to distinguish T_{prog}-like (Ly108+ Cxcr6-) and T_{med}-like (Ly108- Cxcr6+) populations, as done previously[4] (**Fig. 2E**). Supporting the validity of this gating strategy, expression of the stem-like transcription factor TCF1, was higher in Ly108+ Cxcr6- T_{prog}-like than Ly108- Cxcr6+ T_{med}-like -like populations **(Figure S2A).** Further, expression of the CD39 mediator marker[4] was lower in Ly108+ Cxcr6- T_{prog}-like cells than Ly108- Cxcr6+ T_{med}-like populations (**Figure S2B).** Using this gating strategy, a significant increase in T_{prog}-like cells was seen in pLN of *NOD-UTX*^{TCD} mice, compared to *NOD-WT* **(Fig. 2F)**.. At the same time, a significant decrease in T_{med}-like populations was seen in pLN of *NOD-UTX*^{TCD} mice, compared to *NOD-WT.* Taken together, our scRNAseq and flow cytometric analyses support a model in which UTX promotes conversion of CD8+ T cell progenitors to effectors, which then enter the pancreatic islets to destroy beta cells and incite diabetes **(Fig. 2G)**.

UTX controls progenitor to cytolytic effector differentiation in beta cell-specific CD8+ T cells

CD8+ T cells recognizing the pancreatic beta cell antigen IGRP (islet-specific glucose-6-phosphatase catalytic subunit-related protein) are a major pathogenic population in mice and humans with T1D[15,16]. Indeed, Gearty et al., reported that IGRP-specific stem-like progenitors (T_{prog}; Ly108+ CD39-) give rise to both T_{prog} and autoimmune mediator (T_{med}; Ly108- CD39+) populations, and as few as 20 pLN T_{prog} cells from NOD donors can induce diabetes in immunodeficient hosts[3]. Given their potent diabetes-inducing potential, we sought to define the role of UTX in IGRP-specific T_{prog} cells.

In keeping with the markers used by Gearty et al., we identified pLN CD8+ T_{prog} cells as Ly108+ CD39- cells and T_{med} cells as Ly108- CD39+ cells[3] (**Fig. 3A**). As expected, Ly108+ CD39- T_{prog} cells expressed lower levels of the mediator marker CXCR6 than Ly108- CD39+ T_{med} cells **(Fig. 3B)**. We further identified IGRP-specific T cells by their expression of CD44, a marker of antigen-experienced T cells, and their binding to tetramers containing the IGRP mimotope NRP-V7 (CD44+ NRP-V7+)[17]. Using this gating approach, we found that the frequency of T_{prog} cells among IGRP-specific, antigen-experienced CD8+ T cells (Ly108+ CD39- cells within CD8+ CD44+ NRP-V7+) was increased in *NOD-UTX^{TCD}* pLNs compared to *NOD-WT* **(Fig. 3C)**. At the same time, the frequency of T_{med} cells (Ly108- CD39+ cells) within antigen-experienced, IGRP-specific (CD8+ CD44+ NRP-V7+ cells) was significantly lower in *NOD-UTX^{TCD}* pLNs compared to *NOD-WT* **(Fig. 3C)**. Similar findings were seen when CXCR6, rather than CD39, was used as a mediator marker **(Figure S2C)**. Together, these findings demonstrate a role for UTX in promoting conversion of beta cell-specific T_{prog} to T_{med} in the pLN.

To further test UTX's role in beta cell-specific CD8+ T cells, we performed adoptive transfers of IGRP-specific T_{prog} into immunodeficient *NOD.SCID* recipients **(Fig. 3D).** In order to isolate sufficient numbers of IGRP-specific T_{prog} for transfer, we exploited an NOD T cell receptor (TCR) transgenic mouse line (*NOD-TCR 8.3*) in which T cells express a TCR recognizing the $IGRP_{206-214}$ epitope in the context of MHC Class I[18]. IGRP-specific CD8+ T cell progenitors (Ly108+

CD39-) were sorted from 6 week old *NOD-TCR 8.3* mice with or without T cell specific deficiency in UTX (*NOD-TCR 8.3 UTX^{TCD} or NOD-TCR 8.3 WT*, respectively). Five weeks after transfer, an increased frequency of T_{prog} cells (Ly108+ CD39- among CD8+ CD44+) was seen in hosts receiving UTX-deficient CD8+ T_{prog} cells, compared to wildtype **(Fig. 3E)**. Concomitantly, a decrease in the frequency of T_{med} (Ly108- CD39+ among CD8+ CD44+) was noted in recipients of UTX-deficient T_{prog} cells **(Fig. 3E)**. Together, these findings provide further evidence that UTX functions in IGRP-specific CD8+ T_{prog} cells to promote their transition to T_{med} cells.

UTX regulates chromatin accessibility and transcriptional changes in antigen-specific pLN T_{prog} cells

Because UTX is an epigenetic regulator[19], we reasoned that UTX may alter chromatin accessibility (and subsequent gene transcription) in T_{prog} populations to control their conversion to T_{med}. To examine this, we performed concomitant bulk ATAC- and RNA-seq on sort-purified beta cell-specific CD8+ T_{prog} cells from pLN of either *NOD-TCR 8.3 UTX^{TCD}* or *NOD-TCR 8.3 WT* mice.

ATAC-seq analysis demonstrated large-scale chromatin accessibility alterations in UTX-deficient CD8+ T cells. Principal component analysis (PCA) plots showed sample clustering by genotype **(Fig. 4A, top),** highlighting the extensive impact of UTX on the chromatin landscape of CD8+ T cells. RNA-seq analysis done in parallel also showed large-scale transcriptional changes, with PCA analysis of gene expressions demonstrating genotype-specific clustering **(Fig. 4A, bottom)**. Integrative analysis of ATAC- and RNA-seq identified a significant positive correlation (Pearson $R = 0.73$, $p < 2.2 \times 10^{-16}$) of the changes in chromatin accessibility versus gene expression between the genotypes, suggesting that chromatin accessibility and transcription are directly correlated **(Fig. 4B, C)**.

Multiple factors play a key role in the differentiation and maintenance of stem-like progenitor CD8+ T cells, and concurrent changes in chromatin accessibility and transcription were

observed in *NOD-TCR 8.3 UTX^{TCD}* T_{prog} cells. For instance, *NOD-TCR 8.3 UTX^{TCD}* T_{prog} cells demonstrated increased chromatin accessibility, with corresponding increased gene expression, at the *Bcl6* locus **(Fig. 4D and Figure S3A)**, a transcription factor that prolongs stem-like progenitor persistence[20]. Additionally, *NOD-TCR 8.3 UTX^{TCD}* T_{prog} also showed increased chromatin accessibility and gene expression at the *Bach2* locus **(Fig. 4D, E)**, a transcriptional repressor that promotes stem-like CD8+ T cell differentiation programs while suppressing terminal exhaustion programs [20]. Finally, *Bcl2*, an anti-apoptotic factor that promotes stem-like progenitor cell survival[21], also showed increased accessibility and expression in *NOD-TCR 8.3 UTX^{TCD}* T_{prog} cells **(Fig. 4D, E)**. Thus, UTX deficiency is associated with changes at loci important in differentiation and maintenance of stem-like progenitors.

At the same time, decreased accessibility and reduced expression were seen in *NOD-TCR 8.3 UTX^{TCD}* T_{prog} cells at genes important for CD8+ T cell effector function. These genes include cytolytic molecules important in beta cell killing (e.g., *Gzmb, Gzmc, Fas*)[22]; integrins critical in leukocyte islet infiltration (e.g., *Itga4*, *Itgae*)[23,24]; and cytokine/cytokine receptors (e.g., *Ifngr1, Cxcr6*) [4,25,26]. Both *Dapl1* and *Nfatc2,* which function together in CD8+ T cell effector function[27] also were less accessible and expressed. Moreover, genes associated with T cell activation (*Fosl2*[28]*, Thy1*[29]*, Cd9*[30]) were also less accessible and downregulated in expression in CD8+ T cells from *NOD-TCR 8.3 UTX^{TCD}* mice. Gene set enrichment analysis (GSEA) confirmed these patterns for upregulated Stem-Like Progenitor and downregulated Effector gene signatures in *NOD-TCR 8.3 UTX^{TCD}* cells **(Fig. 4F, G; Table S2)**[4,14].

Enrichment analysis of differentially accessible genes revealed association with pathways important in stem-like progenitor generation and cytolytic effector differentiation and function. For instance, Wnt signaling is critical in the generation and maintenance of stem-like memory T cells[31], and Enrichr pathway analysis[32] of differentially accessible genes revealed upregulation of 'Wnt Signaling Pathway' and "Canonical Wnt Signaling Pathway' genes in *NOD-TCR 8.3 UTX^{TCD}* T_{prog} cells **(Figure S3B)**. Additionally, HOMER (Hypergeometric Optimization of Motif

Enrichment) analysis of genes more accessible in *NOD-TCR 8.3 UTX*^{TCD} T_{prog} cells revealed enrichment of motifs associated with *Myb,* a transcription factor essential for generation and maintenance of stem-like memory CD8+ T cells[33] **(Figure S3C).** At the same time, 'Lymphocyte Differentiation', 'Integrin Cell Surface Interactions', 'Positive Regulation of Lymphocyte Activation' and other pathways associated with cytolytic effector function were seen by Enrichr pathway analysis to be downregulated in *NOD-TCR 8.3 UTX*^{TCD} T_{prog} cells **(Figure S3B)**. Together, these findings provide further support that UTX poises chromatin in stem-like T_{prog} cells for transition to cytolytic effectors.

The UTX inhibitor GSKJ4 protects from T1D.

As an epigenetic regulator, UTX functions in part by catalyzing the removal of repressive H3K27me3 (trimethylated histone H3 lysine 27) marks at target loci[19]. UTX's H3K27me3 demethylase activity can be inhibited by a small molecule, GSKJ4[34]. As expected, incubation of NOD mouse CD8+ T cells with GSKJ4 increased H3K27me3 levels (**Fig. 5A)**. As such, UTX may be a druggable target in CD8+ T cells to modulate stem-like progenitor to effector conversion and alter autoimmune responses.

Of note, GSKJ4 has been administered in vivo to mice with minimal toxicity[35]. We therefore exploited this to test the effects of GSKJ4 on T1D development. Administration of GSKJ4 (75 mg/kg i.p. daily for 3 weeks) to 3-week-old NOD females protected mice from diabetes development weeks after treatment was completed **(Fig. 5B)**. Flow cytometric analysis of pLN in mice revealed significantly increased beta cell-specific CD8+ T_{prog} (%Ly108+ CD39- among CD8+ CD44+ NRP-V7+), along with decreased T_{med} (%Ly108- CD39+ among CD8+ CD44+ NRP-V7+) **(Fig. 5C)**. Together, these findings suggest that GSKJ4 treatment prevents CD8+ T_{prog} to T_{med} conversion and T1D development in NOD mice.

UTX blockade alters the distribution of human CD8+ T cell subsets

Recent work has associated T1D in humans with increased circulating CD8+ T memory stem cells (T_{SCM}), a long-lived, self-renewing beta cell-specific population[2,36,37]. T_{SCM} cells play a key role in T1D pathogenesis by giving rise to terminally-differentiated effector/mediator (T_{TE}) cells that ultimately kill insulin-producing beta cells. Thus, during T1D pathogenesis, the T_{SCM} (CCR7+, CD45RA+ CD95+)[36] and T_{TE} population (CCR7- CD45RA+ CD95+)[36] in patients with T1D may have a parallel role to the autoimmune progenitor (T_{prog}) and autoimmune mediator (T_{med}) populations, respectively, in NOD mice[37]. To test whether UTX controls T_{SCM} to T_{TE} conversion, we utilized CRISPR/Cas9 to edit the *UTX* locus in CD8+ T cells isolated from T1D patient peripheral blood mononuclear cells. UTX protein deficiency was validated in CD8+ T cells edited with UTX-targeted single guide RNAs (sgRNAs), compared to negative control (non-targeting control, NTC gRNA) **(Figure S4A)**. After seven-day culture with homeostatic cytokines (IL-2, IL-7, and IL-15) comparison of CD8+ T cell subset distribution revealed an increased frequency of T_{SCM} and a decreased frequency of T_{TE} in UTX-deficient CD8+ T cells compared to the NTC control cells **(Figure S4B)**. This altered distribution supports a cell-intrinsic role for UTX in T_{SCM} to T_{TE} conversion in human CD8+ T cells. Thus, UTX plays a parallel role in CD8+ T cell progenitor to mediator conversion in both mice and humans.

The H3K27me3 demethylase inhibitor GSKJ4 has activity not only in mouse cells, but also in human cells[34]. In line with this report, treatment of human peripheral blood CD8+ T cells indeed increased H3K27me3 levels **(Fig. 5D)**. We therefore exploited GSKJ4 to delineate the role of UTX's demethylase activity in human T1D memory CD8+ T cell differentiation. GSKJ4 treatment of activated CD8+ T cells from T1D patients resulted in accumulation of CD8+ T_{SCM}[22] cells, with a concomitant decrease in T_{TE} **(Fig. 5E)**. Thus, our findings support the role of UTX in promoting human CD8+ T_{SCM} to T_{TE} conversion in T1D and identify UTX as a potential therapeutic target to halt CD8+ T autoimmune effectors.

UTX in T cells is required for anti-PD1 induced T1D

PD1 (programmed death protein) blocking antibodies are widely used to treat a diverse array of cancers, but their immune activating effects can induce T1D and other unwanted autoimmune diseases[38]. Anti-PD1-induced T1D is a rare, but potentially life-threatening, condition for which there is currently no immunotherapeutic therapies[39]. Compared to spontaneous T1D, the clinical course of anti-PD1 induced T1D is accelerated, with rapid destruction of insulin-producing beta cells. At the same time, anti-PD1 induced T1D and spontaneous T1D also have important similarities, including a chronic and unremitting autoimmune T cell response against beta cell antigens. In both conditions, T_{prog} cells play a key role[3,40], and they are believed to be activated directly by anti-PD1 therapy[40,41]. In particular, anti-PD1 promotes transition of beta cell-specific T_{prog} cells to effectors. Whether anti-PD1 induced T1D requires UTX function in T_{prog} cells, however, is unclear.

Anti-PD1 treatment in NOD mice results in accelerated diabetes development and is widely used as an animal model of human anti-PD1 induced T1D [41,42]. We therefore treated *NOD-WT* or *NOD-UTX^{TCD}* mice with anti-PD1 antibody to determine the effects of T cell specific UTX deficiency on the development of anti-PD1-induced T1D. Similar to previous reports[18], all anti-PD1 treated *NOD-WT* mice developed diabetes by 10 days of age. In contrast, *NOD-UTX^{TCD}* mice were protected from diabetes for up to 25 days, at the conclusion of the experiment **(Fig. 6A)**. Histological examination of pancreas sections revealed lower levels of immune infiltrate in anti-PD1-treated *NOD-UTX^{TCD}* mice **(Fig. 6B, C),** and flow cytometric analysis demonstrated decreased numbers of IGRP-specific CD8+ T cells infiltrating the pancreas **(Fig. 6D)**. Moreover, anti-PD1-treated *NOD-UTX^{TCD}* mice showed lower frequency of pLN T_{med} (Ly108- CD39+), and higher frequency of T_{prog} (Ly108+ CD39-), compared to anti-PD1-treated *NOD-WT* controls **(Fig. 6E)**. Together, these data support a model in which UTX-mediated conversion of T_{prog} to cytolytic mediators is required for the development of accelerated anti-PD1 induced T1D **(Fig. 6F).**

Discussion

For patients with T1D, the persistence of the beta cell autoimmune response results in a lifetime of insulin-dependence, predisposition to cardiovascular disease and other T1D-associated complications including shortened life expectancy[43]. Accumulating evidence points to a key role for stem-like progenitor CD8+ T cells in prolonging the autoimmune response[2,3]. Within the pLN of NOD mice, these long-lived cells continually repopulate the pool of terminally-differentiated, cytolytic CD8+ T cells, which then migrate into the pancreas to mediate beta cell destruction. The mechanisms controlling conversion of stem-like memory CD8+ T cells to cytolytic effectors, however, remain incompletely understood. Here, we identify UTX as a critical epigenetic regulator controlling this conversion in both human and mouse cells. Moreover, a small molecule inhibitor of UTX effectively blocked this conversion in both human and mouse cells and protected against T1D in NOD mice. Taken together, these findings suggest that blocking UTX function may be an effective approach to disrupting the T1D autoimmune process.

Although TCF1 is the transcription factor most associated with T_{prog} cells, our data suggest that UTX does not directly regulate the *Tcf7* locus in beta cell-specific T_{prog} cells. Instead, UTX regulates multiple additional factors (*Bcl6, Bach2, Bcl2*) important in differentiation and maintenance of stem-like progenitors. Chromatin accessibility and transcription were increased at these loci in UTX-deficient CD8+ T cells, suggesting that UTX functions to close chromatin and decrease transcription at these loci. In addition, UTX also poises the chromatin structure for increased transcription at multiple effector loci (e.g., *Gzmb, Thy1, Cxcr6*) in CD8+ T_{prog} cells. Thus, UTX has the dual role of repressing transcription at stem-like progenitor loci while promoting gene expression at effector loci.

In addition to spontaneous diabetes, our data indicate that T cell-specific UTX deficiency also protects NOD mice from anti-PD1 induced T1D development. PD-1 blockade is widely used as a cancer immunotherapy, but a major risk with this class of therapies is the development of

unwanted immune related adverse events (IRAEs) [44]. Serious IRAEs include a fulminant, accelerated form of T1D that does not remit and for which there is currently no cure. Previous studies have shown that anti-PD1 treated NOD mice similarly develop accelerated T1D, and this acceleration is associated with increased islet-infiltrating effector-like CD8+ T cells [40,45]. In this study, we show that the diabetes-accelerating effect of anti-PD1 therapy is UTX-dependent. These findings suggest that blocking UTX function may be a potential therapeutic strategy not only in spontaneous T1D, but also in anti-PD1-induced T1D.

It is now clear that non-genetic factors play a key role in T1D pathogenesis. Between 2002-2012, the incidence of T1D in youth increased by 1.4% per year, a rise is too rapid to be attributable to genetics alone[46]. One way in which environmental cues can induce autoimmunity is through environmentally-influenced epigenetic modifications, in which gene expression is altered without changing DNA sequences[47]. Multiple lines of evidence suggest a role for epigenetic regulation of diabetogenic T cells. Most recently, epigenetic regulation of the *Tcf7* locus has been implicated in the expression of TCF1 in diabetogenic CD4+ T cells[12]. Whether epigenetic regulation also controls transcriptional landscape of diabetogenic CD8+ T cells, however, remained unclear. In this study, we show that diabetogenic CD8+ T cells are indeed subject to epigenetic regulation and that the epigenetic regulator UTX is key to controlling conversion of CD8+ T_{prog} to T_{med} cells.

Resource Availability

Lead Contact

Further information and requests for resources and reagents should be directed to and will be fulfilled by the lead contact, Maureen Su (masu@mednet.ucla.edu).

Materials availability

All mouse lines generated in this study will be made available on request from the lead contact.

Data and code availability

Bulk RNA sequencing (GEO: GSE282227) and single-cell RNA sequencing (GEO: GSE283268) data were deposited in the National Center for Biotechnology Information Gene Expression Omnibus database. The paper did not include any original code. Software and packages are listed in the key resources table and method. All scripts of the bioinformatic analyses are available upon request from the lead contact.

Acknowledgments

The authors thank the NIH Tetramer Core (Atlanta, GA) for providing the NRP-V7/H-2Kd PE tetramer. We also thank the Flow Cytometry Core at the University of California, Los Angeles for technical support and the Technology Center for Genomics & Bioinformatics (TCGB) at the University of California, Los Angeles for the help of scRNA-, bulk RNA- and ATAC- sequencing. Finally, the work was funded by NIH U19AI181729 and NIH R01DK119445 to M.A.S.

Author Contributions

H.C.C., M.G.L., W.L., M.A.S. conceptualized the study. H.C.C., S.Z., L.K., Z.Z., and W.H. performed bioinformatics analysis. H.C.C., H.H.W., L.K., D.S., S.Z., E.M., X.Y., J.O., and N.W. performed the experiments. H.C.C., E.M., W.H., M.G.L., and M.A.S. contributed to data visualization. M.A.S. contributed to the original draft. H.C.C., L.K., N.W., M.G.L., W.H., and M.A.S. reviewed and edited the final manuscript.

Declaration of Interests

The authors declare no competing interests.

Figure Legends

Figure 1. Resistance to T1D in *NOD-UTX^{TCD}* mice is associated with altered distribution of pLN CD8+ T cells. A) Diabetes-free incidence curves of *NOD-UTX*^{TCD} vs. *NOD-WT* female littermates. ****p<0.0001; Log rank test. **B and C)** Representative H/E stained pancreas sections (B) and cumulative islet infiltration scores (C) from *NOD-UTX*^{TCD} vs. *NOD-WT* female littermates. *p<0.05, Tukey's multiple comparisons test. **D)** Scheme for 10X genomics single-cell RNA sequencing (scRNAseq) of CD45+ cells from pLN of *NOD-WT* and *NOD-UTX^{TCD}* mice. **E and F)** UMAP of CD45+ (E) and subclustered CD8+ T cells (F). **G)** Gene expression across the CD8+ T cell clusters. **H)** Comparison of subset frequencies of CD8+ T_{prog}-like and CD8+ T_{med}-like populations. CD8+ T_{prog}-like, *p=0.015; CD8+ T_{med}-like, *p=0.026; two-sided, unpaired Mann-Whitney test.

See also Figure S1.

Figure 2. Impaired conversion of stem-like progenitors to effectors in *NOD-UTX^{TCD}* mice. A) UMAP plot of CD8+ T_{prog}-like, CD8+ T Intermediate, and CD8+ T_{med}-like clusters (left), with cells color-coded chronologically along Slingshot pseudotime (right). **B)** Heatmap of scRNAseq expression for key genes, plotted along Slingshot pseudotime. **C)** Expression of key genes along Slingshot pseudotime trajectory, color coded by clusters shown in UMAP (A, left). **D**) Comparison of cell densities of CD8+ T_{prog}-like, CD8+ T Intermediate, and CD8+ T_{med}-like cells derived from 8-week-old *NOD-WT* (WT) vs. *NOD-UTX^{TCD}* (UTX^{TCD}) mice, plotted along Slingshot pseudotime trajectory. Asymptotic two-sample Kolmogorov-Smirnov test, P < 2.2 e-16. **E)** Gating scheme for identifying T_{prog}-like and T_{med}-like cells by flow cytometric analysis. **F)** Representative flow cytometric plot (left) and average frequencies (right) of pLN T_{prog}-like (Ly108+ Cxcr6-) and T_{med}-like (Ly108- CXCR6+) cells of *NOD-WT* and *NOD-UTX*^{TCD} female littermates (12-16 weeks of age). ****p<0.0001; **p<0.01; Student's t test. **G)** Working model:

UTX promotes conversion of long-lived stem-like CD8+ T cell progenitors (T_{prog}) to short-lived mediators (T_{med}), which then enter pancreatic islets to mediate beta cell destruction.

See also Figure S2.

Figure 3. UTX promotes T_{prog} to T_{med} conversion of beta cell-specific CD8+ T cells. A) Gating scheme for identifying T_{prog} and T_{med} cells by flow cytometric analysis. **B)** Representative histogram of CXCR6 expression in T_{prog} vs. T_{med} cell populations identified by Ly108 and CD39 expression. **C)** Representative flow cytometric plot (left) and average frequencies (right) of T_{prog} (Ly108+ CD39-) and T_{med} (Ly108- CD39+) cells within antigen-experienced, IGRP-specific pLN CD8+ T cells (CD8+ CD44+ NRP-V7+) of *NOD-WT* and *NOD-UTX*^{TCD} female littermates (12-16 weeks of age). *p<0.05; Student's t test. **D)** Scheme for adoptive transfer of pLN T_{prog} cells (Ly108+ CD39-) from *NOD-TCR 8.3 WT* vs. *NOD-TCR 8.3 UTX*^{TCD} mice into *NOD.SCID* recipients. **E)** Representative flow cytometric plot (left) and average frequencies (right) of T_{prog} [Ly108+ CD39-] or T_{med} [Ly108- CD39+] among pLN antigen-experienced (CD8+ CD44+) cells in hosts after adoptive transfer as shown in (D). **p<0.01; *p<0.05; Student's t test.

Figure 4. UTX controls chromatin accessibility at progenitor and effector gene loci in antigen-specific pLN T_{prog} cells. A) PCA analysis of ATAC-seq and RNA-seq data from sorted T_{prog} (CD8+ Ly108+ CD39-) from pLN of *NOD-TCR 8.3 WT* and *NOD-TCR 8.3 UTX*^{TCD} CD8+ T_{prog} (n = 3). **B)** Difference in chromatin accessibility of listed genes (in $\log_2$ fold change or FC) between *NOD-TCR 8.3 UTX*^{TCD} and *NOD-TCR 8.3 WT* CD8+ T_{prog} cells as measured by ATAC-seq (decrease accessibility in *NOD-TCR 8.3 UTX*^{TCD}, $\log_2$ FC < -0.5; increased in *NOD-TCR 8.3 UTX*^{TCD}, $\log_2$ FC > 0.5). **C)** Correlation between the differential chromatin accessibility and differential gene expression values (in $\log_2$ FC) in the CD8+ T_{prog} cells of *NOD-TCR 8.3 UTX*^{TCD} compared to *NOD-TCR 8.3 WT* (difference in RNA expression, y-axis; difference in ATAC accessibility, x-axis). R, Pearson correlation coefficient. **D)** Heatmaps of the expression

(left, RNA-seq) and chromatin accessibility (right, ATAC-seq) of selected differentially expressed and accessible genes involved in immune function. The color scale indicates the relative expression or accessibility, with red representing higher values and blue representing lower values. **E)** Representative gene tracks from UCSC Integrated Genome Browser of ATAC-seq, and RNA-seq at indicated gene loci. **F and G)** Gene set enrichment scores for Progenitor signature (Table S2) (F) and Effector signature (G) genes in the *NOD-TCR 8.3 WT* and *NOD-TCR 8.3* UTX^{TCD} CD8+ T_{prog} computed by GSEA.

See also Figure S3.

Figure 5. The UTX inhibitor GSKJ4 protects NOD mice from diabetes and prevents T_{prog} to T_{med} conversion. A) Representative histogram of H3K27me3 levels in NOD CD8+ T cells with and without treatment with the H3K27me3 demethylase inhibitor GSKJ4. **B)** Diabetes-free incidence curve of GSKJ4 (75 mg/kg i.p. daily for 3 weeks starting at 3 weeks of age) vs. vehicle treated female NOD mice**.** *p=0.03, Log rank test. **C)** Representative flow cytometric plot (left) and average frequencies (right) of T_{prog} (Ly108+ CD39-) and T_{med} (Ly108- CD39+) cells within antigen-experienced, IGRP-specific pLN CD8+ T cells (CD8+ CD44+ NRP-V7+) of *NOD-WT* females treated with vehicle (-) vs. GSKJ4 at 20 weeks of age. *p<0.05; Student's t test. **D)** Representative histogram of UTX expression levels in CD8+ T cells from patients with T1D after treatment with vehicle (-) or GSKJ4. **E)** Representative flow cytometric plots (left) and average frequency (right) of T_{SCM} and T_{TE} cells among CD8+ CD95+ peripheral blood cells from T1D patients. Cells were either treated with vehicle control or GSKJ4. *p<0.05, paired Student's t test.

See also Figure S4.

Figure 6. T cell expression of UTX is required for anti-PD1 associated diabetes. A) Diabetes-free incidence curves of anti-PD1 treated *NOD-UTX*^{TCD} vs. *NOD-WT* female

littermates. ****p<0.00001; Log rank test. **B and C)** Representative H/E stained pancreas sections (B) and cumulative islet infiltration scores (C) from anti-PD1-treated *NOD-UTX*^{TCD} vs. *NOD-WT* female littermates, *p<0.05, Chi-square test. **D)** Absolute number of IGRP-specific CD8+ T cells within pancreatic islets of anti-PD1-treated *NOD-UTX*^{TCD} vs. *NOD-WT* female littermates. **p<0.01. Student's t-test. **E)** Average frequency of pLN T_{prog} and T_{med} subsets among CD8+ CD44+ NRP-V7 tetramer+ cells of *NOD-UTX*^{TCD} vs. *NOD-WT* female littermates. Both groups of mice were treated with anti-PD1. ***p<0.001; *p<0.05; Student's t test. **E)** Working model of how UTX is required for the development of anti-PD1 induced T1D, an accelerated form of autoimmune diabetes.

STAR Methods

Mice

NOD/ShiLtJ (NOD;JAX:001976) and NOD.Cg-Prkdc^{scid}/J (*NOD.SCID*; JAX:001303) were purchased from The Jackson Laboratory. *NOD.UTX*$^{fl/fl}$*.LckCre*+ (*NOD-UTX*^{TCD}) was generated by backcrossing *B6.UTX*$^{fl/fl}$*.LckCre*+ mice to NOD mice > 10 generations. We confirmed that the 26 identified diabetes associated (Idd) loci were derived from recipient NOD strain by congenic fine mapping (MegaMUGA). Cre-negative littermates were used as UTX-sufficient, wildtype controls (*NOD-WT*). Only females were included in these studies since UTX is X-linked and expression of the Y-linked homolog UTY in males could confound analyses. *NOD-TCR 8.3 UTX*^{TCD} were generated by crossing *NOD-UTX*^{TCD} mice with NOD.Cg-Tg (TcraTcrbNY8.3)1Pesa/DvsJ (NOD-TCR 8.3; JAX:005868). All mice were housed in a specific pathogen-free barrier facility at UCLA. Experiments were performed in compliance with UCLA Animal Research Committee regulations.

Assessment of diabetes

Mice were monitored for diabetes at least once per week using urine glucose strips (Ascensia Diabetes Care). Mice were considered diabetic after two consecutive urine tests matched with the color of glucose concentration ≥ 250 mg/l.

Anti-PD1 treatment

For anti-PD1 treatment, *NOD-WT* and *NOD-UTX*^{TCD} mice (13 weeks) were injected with anti-mouse PD1 (BioXCell; clone RPM1-14) as previously reported (10mg/kg per dose i.p., twice weekly). Mice are considered diabetic when urine glucose concentration is ≥ 250 mg/dl for two consecutive days.

GSKJ4 treatment

In vivo experiments, three-week-old NOD mice were treated with GSKJ4 (75 mg/kg intraperitoneally) and vehicle (2% DMSO) 5 days/week for 3 consecutive weeks. Mice were monitored for diabetes once per week. Three days or 12 weeks post-treatment, CD8+ T cells were isolated from the pLNs and analyzed by flow cytometry. *In vitro* experiments, human CD8+ T cells were treated with 5nM GSKJ4 (1000x dilution, 5µM as stock) for 72 hours during CD8 T cell stimulation.

Adoptive T cell transfer

All adoptive transfer experiments used NOD.SCID mice as hosts and were performed by intravenous tail vein injections. For CD8+ T cell transfers, splenic CD8+ T cells were isolated by EasySep™ Mouse CD8+ T Cell Isolation Kit (STEMCELL Technologies, #19853), and splenic CD4+ T cells were isolated by EasySep™ Mouse CD4+ T Cell Isolation Kit (STEMCELL Technologies, #19852). $1x10^6$ splenic CD8+ T cells co-transferred with $1x10^6$ splenic CD4+ T cells into the host. Diabetic development was assessed twice a week.

For naïve T cell transfer, naïve CD8 T cells were isolated from the spleen of WT and UTX^{TCD} mice by EasySep™ Mouse Naïve CD8+ T Cell Isolation Kit (STEMCELL Technologies, #19858). $1x10^6$ naïve CD8+ T cells were co-transferred with $1x10^6$ splenic WT CD4+ T cells into the hosts. Three weeks post transfer, pLNs CD8+ T cells were analyzed by flow cytometry.

For CD8+ T_{prog} transfer, Ly108+CD39- among CD8+ CD44+ T_{prog} were sorted from the pLNs of *NOD-TCR 8.3 UTX^{TCD}* or *NOD-TCR 8.3 WT* mice. 250,000 CD8+ T_{prog} were co-transferred with $1x10^6$ splenic WT CD4+ T cells into the hosts. Three weeks post transfer, pLNs CD8+ T cells were analyzed by flow cytometry.

Histology and insulitis scoring

Hematoxylin and eosin (H&E) staining of pancreas tissues are done by UCLA Translational Pathology Core Laboratory (TPCL). Insulitis for each pancreatic islet is scored based on percent of islet infiltrated by immune cells: 0 = no infiltration, 1 = 0 – 25% infiltration, 2 = 25 – 50% infiltration, 3 = 50 – 75% infiltration, 4 = 75 – 100% infiltration.

Immune cell isolation

Mice were euthanized by CO2. Lymph nodes and spleens were mechanically disrupted with the back of 1-ml syringe, filtered through a 40-µm strainer, and performed ACK lysis for 1 min. Cells were washed once with PBS. Pancreas digestion was adapted from existing protocols. In brief, 3 ml of collagenase type IV solution (2mg/ml) with DNaseI (10U/ml) in HBSS (Gibco 14025-092) supplemented with 10% fetal bovine serum (FBS) and DNaseI (10U/ml) was injected into the clamped pancreatic duct. Perfused pancreases were then excised and incubated in 4 ml of the collagenase solution at 37^{o}C for 30 min. The digested pancreas was then washed using 10mL HBSS with 10% FBS and spun down at 300g for 3 min, 2 times, followed by mechanically breaking up the pancreas. Then, tissue was passed through a 40-µm strainer and washed with

HBSS with 10% FBS, and spun down at 400g for 5 min. Finally, the pellet was resuspended into FACS buffer for antibody staining.

Surface staining for flow cytometry and cell sorting

Cells were analyzed for surface markers using fluorophore-conjugated antibodies. Cell surface staining was performed in FACS buffer (2% FBS and 2mM EDTA in PBS) for 30 min at 4^{o}C. Intranuclear protein staining, including UTX, H3K27me3, and TCF1, was performed by fixing and permeabilizing using the eBioscience Foxp3/Transcription Factor kit. Followed by the primary rabbit antibody, Goat Anti-Rabbit IgG H&L (Abcam) was used as the secondary antibody.

H-2Kd/NRP-V7 (KYNKANFL) tetramer was obtained from the NIH Tetramer Core Facility. Tetramer staining was performed with two steps: cells were stained with tetramer in PBS solution (1:200) for 30 min at room temperature, followed by staining with surface markers for 30 min at 4^{o}C. Flow cytometry was performed on an LSRII Fortessa and FACS sorting was performed on an ARIA or ARIA-H instrument (BD Biosciences, San Jose, CA) at the UCLA Broad Stem Cell Research Center Flow Cytometry Core. The data were analyzed with FlowJo v10.7.2 (TreeStar).

Single cell RNA analysis

Pancreatic lymph node (pLN) scRNAseq data are clustered using Seurat package (version 4.4.0). Differential gene markers of each cluster are computed using the FindAllMarkers function of Seurat. Immune cell types are defined based on their canonical markers (Table S1A). Cd8 T cell clusters, including clusters with mixed Cd8 and Cd4 T cells, are re-integrated after updating their list of variable genes, scaled, and reclustered (Table S1B). Clusters containing cells with high mitochondrial, ribosomal, and non-coding RNAs are deemed to be low quality and are

removed from our subsequent analyses. The clustering of Cd4 T cells is performed in the same manner (cluster markers in Table S1C).

Uniform manifold approximation and projection (UMAP) plots, violin plots, dot plots, boxplots visualizations are done using functions from Seurat package or ggplot2 package (version 3.5.1). Cell count frequency is calculated by normalizing cell count from each cluster to the total cell count of a specified cell type (e.g. Cd8 T cells or Cd4 T cells) in each sample. Pseudotime analysis is performed using Slingshot package (version 2.4.0). Heatmaps are generated using ComplexHeatmap package (2.12.1)

Isolation of human CD8+ T cells

This study was conducted with approval from the institutional review boards of the University of California, Los Angeles (UCLA): written informed consent was obtained. All donors included in this study were female. For adult donors with T1D, blood was collected through UCLA endocrine clinics. For healthy adult donors, blood was collected through the UCLA Virology Core Laboratory. Collected blood was then performed peripheral blood mononuclear cell isolation, diluted with sterile PBS (Thermo Fisher Scientific). 35 mL of diluted blood was then overlayed with 15 mL of Ficoll-paque (GE Healthcare). The gradient was centrifuged at 400g with no brake for 30 min at room temperature. The PBMC interphase layer was collected, washed with FACS buffer, and centrifuged at 400g for 5 min, and cryopreserved in liquid nitrogen. For CD8+ T cell stimulation, PBMC CD8+ T cells were enriched with EasySep™ Human CD8+ T Cell Isolation Kit (STEMCELL Technologies, #17953).

T cell stimulation

Mouse and human CD8+ T cells ($1x10^6$/mL) were cultured in 10% FBS completed RPMI + human IL-2 (50 U/ml). Medium for mouse CD8+ T cells culture was supplemented with 1x 2-

Mercaptoethanol (Gibco, 21985023). CD8+ T cells were plated in 48-well non-tissue culture plate or stimulation. Mouse CD8+ T cells were stimulated by Dynabeads™ Mouse T-Activator CD3/CD28 and human CD8+ T cells were stimulated by Dynabeads™ Human T-Activator CD3/CD28. After stimulation, mouse and human CD8+ T cells were analyzed by intracellular and surface protein staining.

RNA-seq library construction and data processing

Total RNA was isolated from sort-purified CD8+ progenitors (Ly108+CD39-) using Quick RNA MiniPrep Kit (Zymo). RNA quality was verified using TapeStation analysis. RNA-seq libraries were generated by UCLA Technology Center for Genomics & Bioinformatics (TCGB) and sequenced on a Novaseq X Plus (paired-end, 2x50 bp). RNA-seq analysis was carried out by first checking the quality of the reads using FastQC. Then, they were mapped with HISAT2 (version 2.2.1) to the mouse genome (mm10). The counts for each gene were obtained by featureCounts package. Differential expression analyses were carried out using DESeq2 (version 1.24.0) with default parameters. Genes with absolute fold change difference of > 1.5 with an FDR-adjusted P value < 0.05 were considered significantly differentially expressed.

ATAC-seq library construction and data processing

CD8+ progenitors (Ly108+CD39-) isolated from the pLNs of *NOD-TCR 8.3 WT* (n=3) and *NOD-TCR 8.3 UTX*^{TCD} (n=3) mice were purified by cell sorting. Each genotype has 3 biological replicates. 50,000 cells were used for ATAC-seq library preparation based on published Omni-ATAC protocol[48]. In brief, the sorted cells were treated with lysis buffer for 3 min on ice, and the extracted nuclei were resuspended in the transposition mix containing 2.5 ul transposase (Illumina) and incubated at 37^{o}C for 30 min with 1,000 rpm shaker. The products were purified with DNA Clean and Concentrator-5 Kit (Zymo Research) and then amplified with PCR for 11

cycles using barcoding primers provided by previous literature. PCR products were performed size selection using AMPure XP Bead (Beckman coulter) to purify DNA fragments from 150-1,000 bp. The concentration and quality control were measured by Qubit and Tapestation. The libraries were pooled based on molar concentrations and sequenced on Novaseq X Plus (paired-end, 2x50 bp).

The sequencing quality of the libraries was assessed by *FastQC* (0.11.9), followed by the trimming process using *Cutadapt* (4.6). *Bowtie2* (2.4.2) was used to align the sequencing reads to the mm10 mouse genome, and only uniquely mapped reads (MAPQ≥30) were retained for downstream. *SAMtools* (1.15.0) was used to convert SAM files into BAM files and sort BAM files. *Picard MarkDuplicates* (2.25) was used to remove duplicate reads in the BAM files. *MACS2* (2.2.9) was used for ATAC-seq peak calling (paired-end mode, FDR-adjusted $q < 0.01$). For differential binding analysis, we used *Diffbind* (3.20) package to determine differentially bound peaks found in all replicates for WT vs UTX^{TCD} with DESeq2 method. Peaks/regions identified as differentially accessible were annotated using the annotatepeaks.pl function from the HOMER analysis package. FeatureCounts Package (2.0.3) was used to count the number of reads that overlap each peak per sample. Chromatin regions were considered as significantly differentially accessible at a threshold of absolute log2 fold change difference in accessibility > 0.5 and FDR adjusted $P < 0.05$. Count-per-million-normalized bigwig files were generated for visualization using *deeptools'* (3.5.6) bamCoverage function. Figures of coverage tracks were exported from bigwig read alignment files using the UCSC Genome Browser. HOMER package was used to find transcriptional factor binding motifs that are enriched in regions with significant differences in chromatin accessibility.

Statistical analysis

Statistical analysis was performed using GraphPad Prism 9 or R for scRNA sequencing analysis. Unpaired t tests were used to compare two groups while paired t tests were used for

matched samples. For type 1 diabetic incidence curves, a log-rank (Mantel-Cox) test was used. Benjamini-Hochberg (also known as FDR method) adjusted p-values were reported for differentially expressed genes, for Pathway Analysis by Enrichr and gene set enrichment analysis by GSEA. Fold changes were calculated as (B-A)/A. A p-value of less than 0.05 was considered significant and data are presented as mean±SEM with the following symbols: *p<0.05, **p<0.01, *** p<0.001.

Excel table titles:

Table S1. Differential expression genes in each cluster of scRNA-seq dataset, related to STAR Methods-Single Cell RNA Analysis

Table S2. CD8+ T stem cell-like memory signature, related to Figure 4

REFERENCES

1 Bluestone, J. A., Herold, K. & Eisenbarth, G. Genetics, pathogenesis and clinical interventions in type 1 diabetes. *Nature* **464**, 1293-1300 (2010). https://doi.org/10.1038/nature08933

2 Abdelsamed, H. A. *et al.* Beta cell-specific CD8+ T cells maintain stem cell memory-associated epigenetic programs during type 1 diabetes. *Nature Immunology* **21**, 578-587 (2020). https://doi.org/10.1038/s41590-020-0633-5

3 Gearty, S. V. *et al.* An autoimmune stem-like CD8 T cell population drives type 1 diabetes. *Nature* **602**, 156-161 (2022). https://doi.org/10.1038/s41586-021-04248-x

4 Ciecko, A. E. *et al.* Self-Renewing Islet TCF1(+) CD8 T Cells Undergo IL-27-Controlled Differentiation to Become TCF1(-) Terminal Effectors during the Progression of Type 1 Diabetes. *J Immunol* **207**, 1990-2004 (2021). https://doi.org/10.4049/jimmunol.2100362

5 Collier, J. L., Weiss, S. A., Pauken, K. E., Sen, D. R. & Sharpe, A. H. Not-so-opposite ends of the spectrum: CD8(+) T cell dysfunction across chronic infection, cancer and autoimmunity. *Nat Immunol* **22**, 809-819 (2021). https://doi.org/10.1038/s41590-021-00949-7

6 Gebhardt, T., Park, S. L. & Parish, I. A. Stem-like exhausted and memory CD8(+) T cells in cancer. *Nat Rev Cancer* **23**, 780-798 (2023). https://doi.org/10.1038/s41568-023-00615-0

7 Pace, L. *et al.* The epigenetic control of stemness in CD8 $^{+}$ T cell fate commitment. *Science* **359**, 177-186 (2018). https://doi.org/10.1126/science.aah6499

8 Mitchell, J. E. *et al.* UTX promotes CD8+ T cell-mediated antiviral defenses but reduces T cell durability. *Cell Reports* **35**, 108966 (2021). https://doi.org/10.1016/j.celrep.2021.108966

9 Noda, H. *et al.* The histone demethylase Utx controls CD8(+) T-cell-dependent antitumor immunity via epigenetic regulation of the effector function. *Cancer Sci* **114**, 2787-2797 (2023). https://doi.org/10.1111/cas.15814

10 Cheng, Y. *et al.* Targeting epigenetic regulators for cancer therapy: mechanisms and advances in clinical trials. *Signal Transduct Target Ther* **4**, 62 (2019). https://doi.org/10.1038/s41392-019-0095-0

11 Cook, K. D. *et al.* T Follicular Helper Cell-Dependent Clearance of a Persistent Virus Infection Requires T Cell Expression of the Histone Demethylase UTX. *Immunity* **43**, 703-714 (2015). https://doi.org/10.1016/j.immuni.2015.09.002

12 Aljobaily, N. *et al.* Autoimmune CD4(+) T cells fine-tune TCF1 expression to maintain function and survive persistent antigen exposure during diabetes. *Immunity* (2024). https://doi.org/10.1016/j.immuni.2024.09.016

13 Anderson, M. S. & Bluestone, J. A. The NOD mouse: a model of immune dysregulation. *Annu Rev Immunol* **23**, 447-485 (2005). https://doi.org/10.1146/annurev.immunol.23.021704.115643

14 Zehn, D., Thimme, R., Lugli, E., de Almeida, G. P. & Oxenius, A. 'Stem-like' precursors are the fount to sustain persistent CD8(+) T cell responses. *Nat Immunol* **23**, 836-847 (2022). https://doi.org/10.1038/s41590-022-01219-w

15 Coppieters, K. T. *et al.* Demonstration of islet-autoreactive CD8 T cells in insulitic lesions from recent onset and long-term type 1 diabetes patients. *J Exp Med* **209**, 51-60 (2012). https://doi.org/10.1084/jem.20111187

16 Gu, M. *et al.* NF-kappaB-inducing kinase maintains T cell metabolic fitness in antitumor immunity. *Nat Immunol* **22**, 193-204 (2021). https://doi.org/10.1038/s41590-020-00829-6

17 Lieberman, S. M. *et al.* Identification of the beta cell antigen targeted by a prevalent population of pathogenic CD8+ T cells in autoimmune diabetes. *Proc Natl Acad Sci U S A* **100**, 8384-8388 (2003). https://doi.org/10.1073/pnas.0932778100

18 Verdaguer, J. *et al.* Spontaneous autoimmune diabetes in monoclonal T cell nonobese diabetic mice. *J Exp Med* **186**, 1663-1676 (1997). https://doi.org/10.1084/jem.186.10.1663

19 Van der Meulen, J., Speleman, F. & Van Vlierberghe, P. The H3K27me3 demethylase UTX in normal development and disease. *Epigenetics* **9**, 658-668 (2014). https://doi.org/10.4161/epi.28298

20 Yao, C. *et al.* BACH2 enforces the transcriptional and epigenetic programs of stem-like CD8(+) T cells. *Nat Immunol* **22**, 370-380 (2021). https://doi.org/10.1038/s41590-021-00868-7

21 Chen, Z. *et al.* TCF-1-Centered Transcriptional Network Drives an Effector versus Exhausted CD8 T Cell-Fate Decision. *Immunity* **51**, 840-855 e845 (2019). https://doi.org/10.1016/j.immuni.2019.09.013

22 Thomas, H. E., Trapani, J. A. & Kay, T. W. The role of perforin and granzymes in diabetes. *Cell Death Differ* **17**, 577-585 (2010). https://doi.org/10.1038/cdd.2009.165

23 Uniyal, S., Boeters, L., Chakrabarti, S., Singh, B. & Chan, B. M. Leukocytes utilize both alpha4 and alpha5 integrins for intraislet infiltration in non-obese diabetic mice. *J Autoimmun* **12**, 167-176 (1999). https://doi.org/10.1006/jaut.1998.0268

24 Barrie, E. S. *et al.* Role of ITGAE in the development of autoimmune diabetes in non-obese diabetic mice. *J Endocrinol* **224**, 235-243 (2015). https://doi.org/10.1530/JOE-14-0396

25 Carrero, J. A., Benshoff, N. D., Nalley, K. & Unanue, E. R. Type I and II Interferon Receptors Differentially Regulate Type 1 Diabetes Susceptibility in Male Versus Female NOD Mice. *Diabetes* **67**, 1830-1835 (2018). https://doi.org/10.2337/db18-0331

26 Kim, C. H. *et al.* Bonzo/CXCR6 expression defines type 1–polarized T-cell subsets with extralymphoid tissue homing potential. *Journal of Clinical Investigation* **107**, 595-601 (2001). https://doi.org/10.1172/jci11902

27 Zhu, L. *et al.* Dapl1 controls NFATc2 activation to regulate CD8(+) T cell exhaustion and responses in chronic infection and cancer. *Nat Cell Biol* **24**, 1165-1176 (2022). https://doi.org/10.1038/s41556-022-00942-8

28 Renoux, F. *et al.* The AP1 Transcription Factor Fosl2 Promotes Systemic Autoimmunity and Inflammation by Repressing Treg Development. *Cell Rep* **31**, 107826 (2020). https://doi.org/10.1016/j.celrep.2020.107826

29 Haeryfar, S. M. M. & Hoskin, D. W. Thy-1: More than a Mouse Pan-T Cell Marker. *The Journal of Immunology* **173**, 3581-3588 (2004). https://doi.org/10.4049/jimmunol.173.6.3581

30 Tai, X. G. *et al.* A role for CD9 molecules in T cell activation. *J Exp Med* **184**, 753-758 (1996). https://doi.org/10.1084/jem.184.2.753

31 Gattinoni, L. *et al.* Wnt signaling arrests effector T cell differentiation and generates CD8+ memory stem cells. *Nat Med* **15**, 808-813 (2009). https://doi.org/10.1038/nm.1982

32 Kuleshov, M. V. *et al.* Enrichr: a comprehensive gene set enrichment analysis web server 2016 update. *Nucleic Acids Res* **44**, W90-97 (2016). https://doi.org/10.1093/nar/gkw377

33 Gautam, S. *et al.* The transcription factor c-Myb regulates CD8(+) T cell stemness and antitumor immunity. *Nat Immunol* **20**, 337-349 (2019). https://doi.org/10.1038/s41590-018-0311-z

34 Kruidenier, L. *et al.* A selective jumonji H3K27 demethylase inhibitor modulates the proinflammatory macrophage response. *Nature* **488**, 404-408 (2012). https://doi.org/10.1038/nature11262

35 Pan, Y. *et al.* GSKJ4 Protects Mice Against Early Sepsis via Reducing Proinflammatory Factors and Up-Regulating MiR-146a. *Front Immunol* **9**, 2272 (2018). https://doi.org/10.3389/fimmu.2018.02272

36 Galletti, G. *et al.* Two subsets of stem-like CD8(+) memory T cell progenitors with distinct fate commitments in humans. *Nat Immunol* **21**, 1552-1562 (2020). https://doi.org/10.1038/s41590-020-0791-5

37 Gattinoni, L., Speiser, D. E., Lichterfeld, M. & Bonini, C. T memory stem cells in health and disease. *Nature Medicine* **23**, 18-27 (2017). https://doi.org/10.1038/nm.4241

38 Cook, S. *et al.* Immune-Related Adverse Events and Survival Among Patients With Metastatic NSCLC Treated With Immune Checkpoint Inhibitors. *JAMA Netw Open* **7**, e2352302 (2024). https://doi.org/10.1001/jamanetworkopen.2023.52302

39 Akturk, H. K. *et al.* Immune checkpoint inhibitor-induced Type 1 diabetes: a systematic review and meta-analysis. *Diabetic Medicine* **36**, 1075-1081 (2019). https://doi.org/https://doi.org/10.1111/dme.14050

40 Collier, J. L. *et al.* Single-cell profiling reveals unique features of diabetogenic T cells in anti-PD-1-induced type 1 diabetes mice. *J Exp Med* **220** (2023). https://doi.org/10.1084/jem.20221920

41 Im, S. J. *et al.* Defining CD8+ T cells that provide the proliferative burst after PD-1 therapy. *Nature* **537**, 417-421 (2016). https://doi.org/10.1038/nature19330

42 Hu, H., Zakharov, P. N., Peterson, O. J. & Unanue, E. R. Cytocidal macrophages in symbiosis with CD4 and CD8 T cells cause acute diabetes following checkpoint blockade of PD-1 in NOD mice. *Proc Natl Acad Sci U S A* **117**, 31319-31330 (2020). https://doi.org/10.1073/pnas.2019743117

43 Arffman, M., Hakkarainen, P., Keskimaki, I., Oksanen, T. & Sund, R. Long-term and recent trends in survival and life expectancy for people with type 1 diabetes in Finland. *Diabetes Res Clin Pract* **198**, 110580 (2023). https://doi.org/10.1016/j.diabres.2023.110580

44 Sharpe, A. H. & Pauken, K. E. The diverse functions of the PD1 inhibitory pathway. *Nat Rev Immunol* **18**, 153-167 (2018). https://doi.org/10.1038/nri.2017.108

45 Perdigoto, A. L. *et al.* Immune cells and their inflammatory mediators modify beta cells and cause checkpoint inhibitor-induced diabetes. *JCI Insight* **7** (2022). https://doi.org/10.1172/jci.insight.156330

46 Hasham, A. & Tomer, Y. The recent rise in the frequency of type 1 diabetes: who pulled the trigger? *J Autoimmun* **37**, 1-2 (2011). https://doi.org/10.1016/j.jaut.2011.04.001

47 Richardson, B. Primer: epigenetics of autoimmunity. *Nat Clin Pract Rheumatol* **3**, 521-527 (2007). https://doi.org/10.1038/ncprheum0573

48 Corces, M. R. *et al.* An improved ATAC-seq protocol reduces background and enables interrogation of frozen tissues. *Nat Methods* **14**, 959-962 (2017). https://doi.org/10.1038/nmeth.4396

Figure 1 Resistance to T1D in *NOD-UTX*^{TCD} mice is associated with altered distribution of pLN CD8+ T cells.

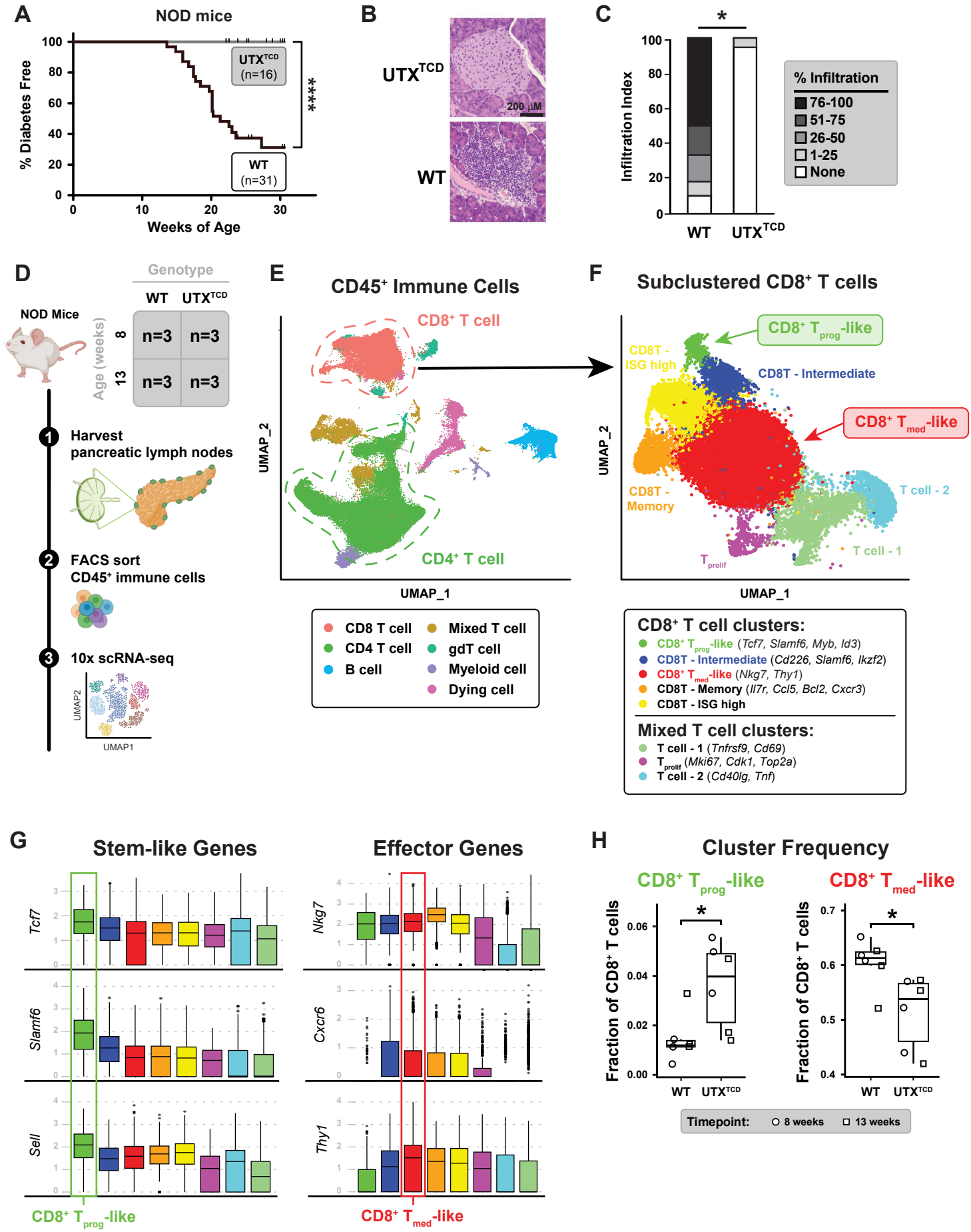

Figure 2. Impaired conversion of stem-like progenitors to effectors in *NOD-UTX*^{TCD} mice.

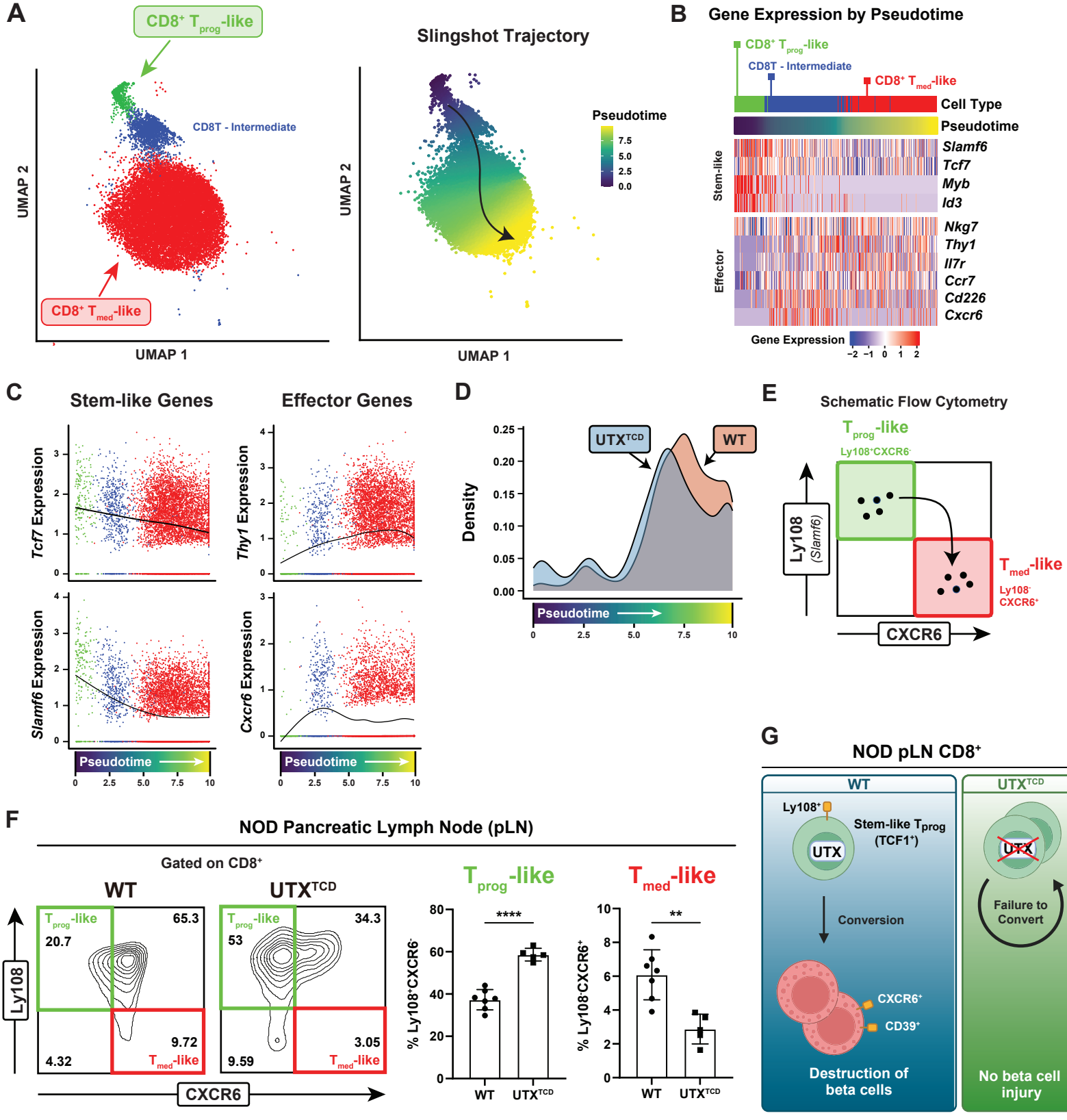

Figure 3. UTX promotes Tprog to Tmed conversion of beta cell-specific CD8⁺ T cells.

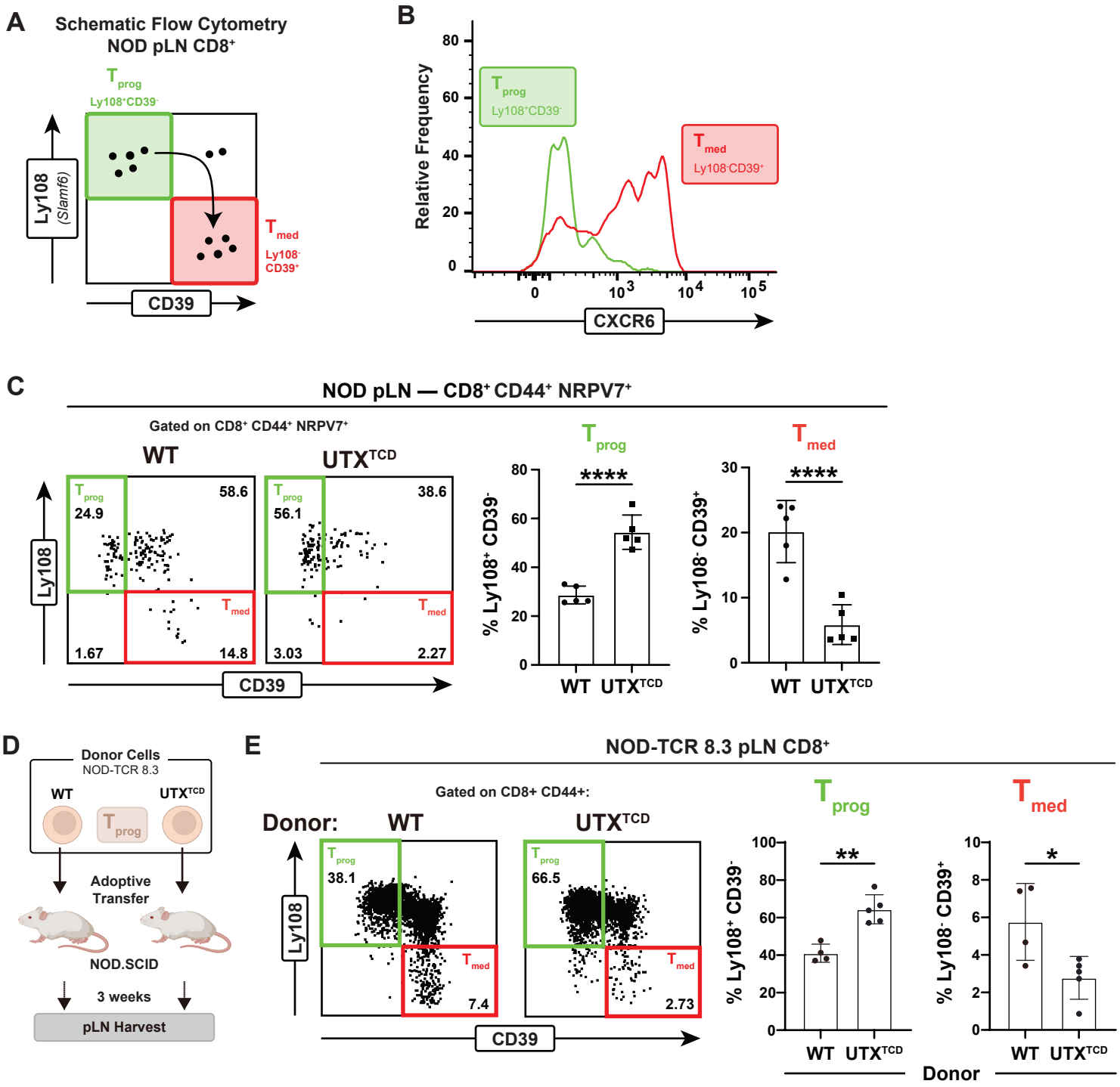

Figure 4. UTX controls chromatin accessibility at progenitor and effector gene loci in antigen-specific pLN Tprog cells.

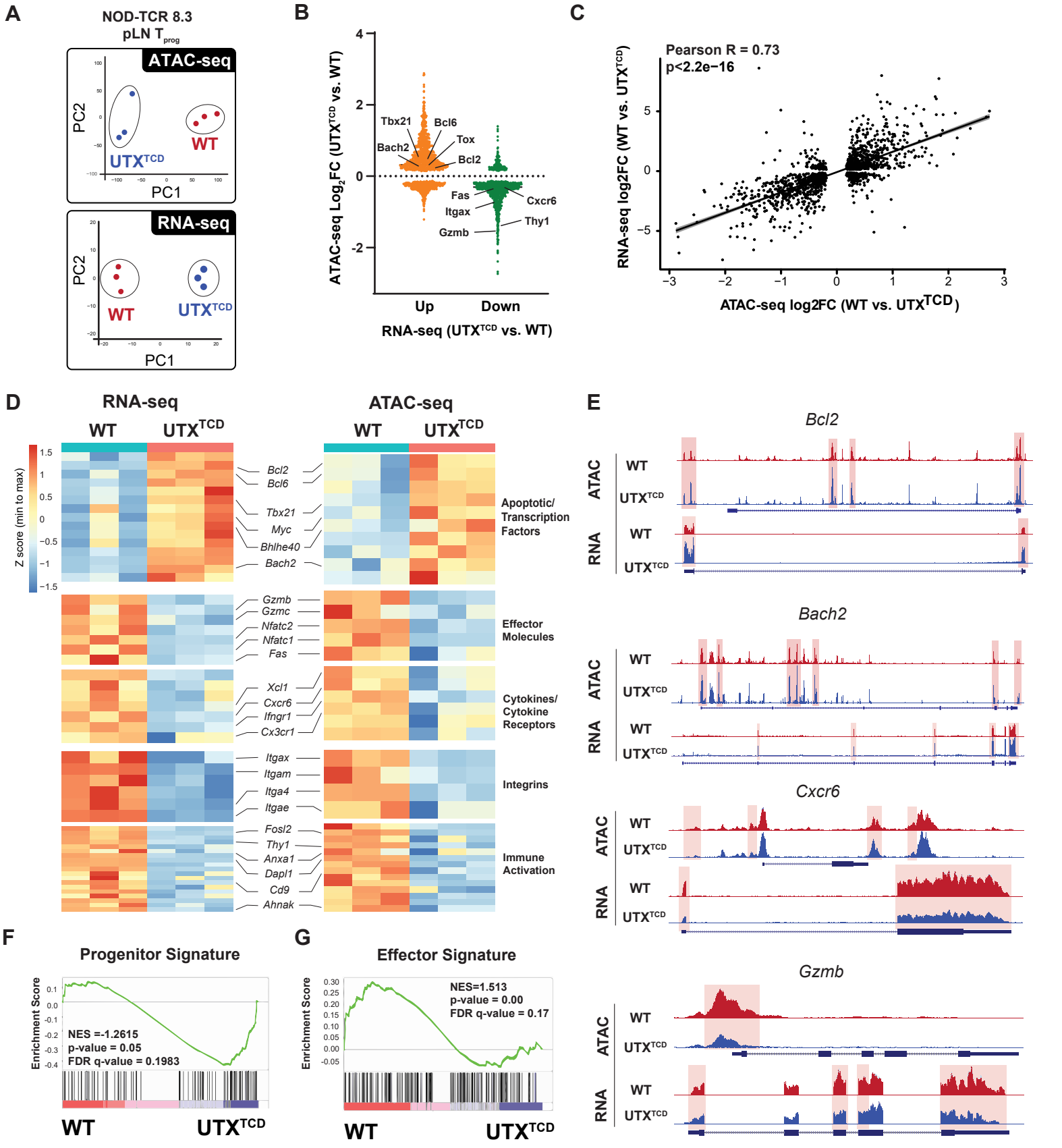

Figure 5. The UTX inhibitor, GSKJ4, protects NOD mice from diabetes and prevents T_{prog} to T_{med} conversion.

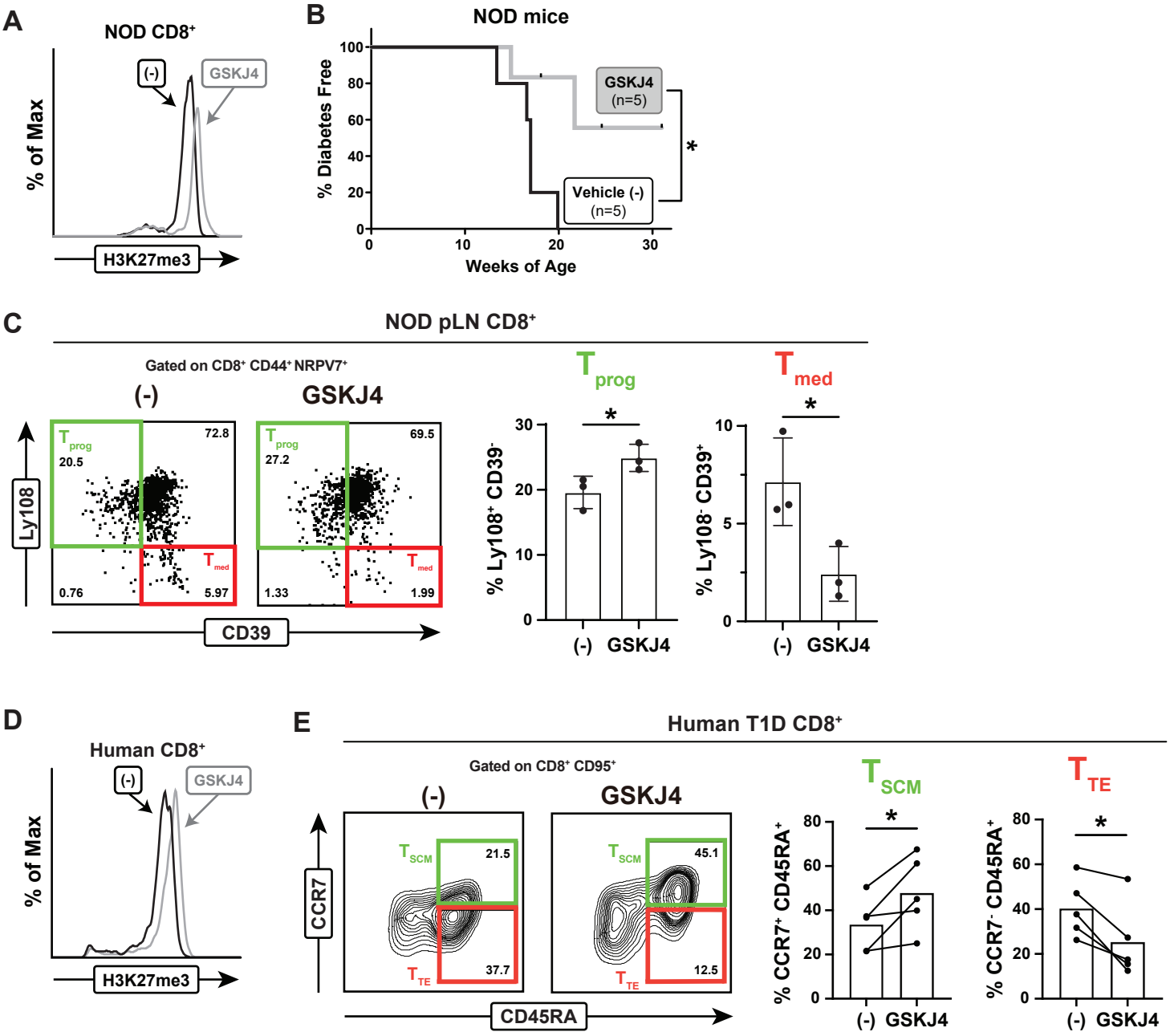

Figure 6. T cell expression of UTX is required for anti-PD1 associated diabetes.